

Article

Study on the Influence of Different Factors on Pneumatic Conveying in Horizontal Pipe

Chengming Wang ^{1,*}, Wenqi Li ¹, Baojun Li ^{2,*} , Zezhong Jia ¹, Shihui Jiao ¹ and Hao Ma ¹¹ School of Mechanical and Power Engineering, Zhengzhou University, Zhengzhou 450001, China² School of Chemistry, Zhengzhou University, Zhengzhou 450001, China

* Correspondence: hitwcm@zzu.edu.cn (C.W.); lbjfc1@zzu.edu.cn (B.L.)

Abstract: Aiming at the problems of high energy consumption and particle breakage in the pneumatic conveying process of large-scale breeding enterprises, in this paper, based on the theoretical calculated value of particle suspension velocity, a computational fluid model and a discrete element model are established based on computational fluid dynamics (CFD) and discrete element method (DEM). Then, through the numerical simulation of gas-solid two-phase flow, the influence of four factors of conveying wind speed, particle mass flow rate, pipe diameter, and particle size on the velocity distribution of particles in a horizontal pipe, dynamic pressure change in the pipe, pressure drop in the pipe, and solid mass concentration are studied. The results show that the $k-\varepsilon$ turbulence model can better simulate the movement of gas-solid two-phase flow, and through the analysis of the simulation, the influence of four different factors on the conveying characteristics is obtained, which provides a scientific basis for the construction of the conveying line.

Keywords: pneumatic conveying; gas-solid coupling; conveying wind speed; particle mass flow rate; conveying characteristics



Citation: Wang, C.; Li, W.; Li, B.; Jia, Z.; Jiao, S.; Ma, H. Study on the Influence of Different Factors on Pneumatic Conveying in Horizontal Pipe. *Appl. Sci.* **2023**, *13*, 5483. <https://doi.org/10.3390/app13095483>

Academic Editors: Hasan Sajjadi and Gholamreza Kefayati

Received: 19 March 2023

Revised: 9 April 2023

Accepted: 26 April 2023

Published: 28 April 2023



Copyright: © 2023 by the authors. Licensee MDPI, Basel, Switzerland. This article is an open access article distributed under the terms and conditions of the Creative Commons Attribution (CC BY) license (<https://creativecommons.org/licenses/by/4.0/>).

1. Introduction

With the rapid development of the world economy, large-scale breeding enterprises are also constantly realizing their own economy through technological innovation. However, for a long time, the breeding industry has been facing various problems such as energy consumption and environmental pollution. Bin Xie et al. [1] used the stable isotopic values of SPOM to label suspended particulate organic matter in dense cage culture to assess the level of water pollution. Gizachew Hailegebreal et al. [2] studied the morbidity and mortality of chickens in poultry farms, concluding that infectious diseases were the main constraint to increasing chicken production. Uri Yogev et al. [3] conducted research on phosphorus residues in aquaculture, and achieved sustainable reuse of phosphorus through phosphorus recovery and avoided environmental pollution. However, there are not only environmental and energy problems in pig breeding, but also feed transportation problems, how to ensure dry and complete pellet feed while taking into account the clean conveying is also one of the economic problems faced by the development of enterprises, so finding a suitable conveying mechanism is particularly important for enterprises. Currently, with the continuous development of conveying technology, pneumatic conveying with air flow as power source is increasingly used by some industries, especially the large-scale breeding industry [4–6], which greatly improves the economy of enterprises.

Traditional large-scale breeding enterprises commonly used particle feedstuff transportation mode with a stopper conveyor and screw conveyor [7–9]; although they can achieve sealed transportation, they cause component wear, particle breakage, and other shortcomings in the conveying process, which increases the cost in the conveying process and is not conducive to the long-term development of large breeding enterprises, so these devices are gradually eliminated. Compared with the traditional mechanical transportation

mode, the pneumatic conveying device has the advantages of simple structure, convenient operation, and high conveying efficiency. The device is not limited by the site and can realize long-distance and multi-directional transportation. In recent years, large-scale breeding enterprises have adopted this transportation mode. The initial application of pneumatic conveying technology was proposed by Medhurst in 1810 to use pipes for pneumatic conveying of mail, and D.F. Othmer [10] studied fluidization in 1956. Then, R.D. Marcus [11] and others gave a detailed introduction to the working principle of pneumatic conveying and conveying characteristics, which deepened people's understanding of pneumatic conveying. Mills et al. [12] provided a large number of practical data for the design of pneumatic conveying system through the analysis of actual cases and theoretical research, laying a foundation for the large-scale development of pneumatic conveying equipment. Reinauer [13] analyzed the sanitary and economic advantages of pneumatic conveying, laying a foundation for the large-scale use of pneumatic conveying. Liansuo An [14] introduced an acoustic emission monitoring system into a pneumatic conveying device, therefore improving the accuracy of monitoring pneumatic conveying devices.

Pneumatic conveying is an air-powered transportation method mainly for granular materials. In the conveying process, the energy consumption is high, and the materials are also easy to break, which affects the economy of enterprises. Therefore, scholars are required to find scientific and reasonable design methods to develop pneumatic conveying systems suitable for particle materials with low energy consumption and high efficiency [15–18]. At the early stage of the development of pneumatic conveying technology, Cornish and Pinkus Oscar [19,20] and others studied the pressure drop in the pipe of pneumatic conveying. Fadeev, Bikbaev, and Bahmani Sina [21–23] studied friction and wear in pneumatic conveying. Gorshkov [24] studied the collision between particles and pipeline wall in pneumatic conveying. With the deepening of the understanding of pneumatic conveying theory, scholars have also improved the pneumatic conveying equipment through research, among which Lodes Antonin et al. [25] optimized the energy consumption in pneumatic conveying. J. Li et al. [26] developed an experimental technique for analyzing the plug flow in pneumatic conveying pipelines by using pressure measurement. Wonsik Chung [27] optimized the garbage pneumatic conveying system based on the facility diagnosis results. Niranjana Behera et al. [28] established a mathematical model of solid friction coefficient, which realized a low error to predict the pressure drop of the pneumatic conveying system.

With the development of computer technology, CFD numerical simulation method is often used in fluid analysis. In recent years, by using the CFD-DEM coupling method, Guanguo Ma et al. [29] simulated a gas-solid two-phase flow of concrete ejection motion in pipe with different ratio of bending diameter, Wenlei Liu et al. [30] studied the radial velocity of soybean under vertical pressure and the resulting pressure drop, and Rong Xue et al. [31] analyzed the energy loss of a low specific speed pump with a fully sealed structure. Some scholars have also solved some problems in pneumatic conveying by using CFD numerical analysis method. For example, Ghafori H. [32] and others proposed a new type of elbow with auxiliary air equipment, and verified by experiments that the average pressure drop of the elbow with a 45° auxiliary air elbow was small, the collision between the particles and the wall surface was less, and particle fragmentation was reduced, but the cost and life of the elbow when used on an industrial scale are not verified. Ying Wang et al. [33] analyzed the bypass pneumatic conveying gas-solid two-phase flow model, compared the pressure drop results of multiple experimental cases and numerical models to prove the applicability and effectiveness of the pressure drop prediction model, but ignored the particle characteristics such as permeability, degassing, particle size distribution, and particle shape in this study. Hasan Ghafori et al. [34] proposed a new technology of porous double pipe, which used an additional air injection system in the pipe to compensate for the pressure drop and verified the reliability of porous double pipe through experiments. However, this technology consumes more materials in long-distance conveying, which reduces the economy. Daolong Yang [35] analyzed the effects of particle size, flow rate, solid gas ratio, and pipe diameter on wall wear through multi-factor simulation, providing

a simulation reference and designing guidance for pneumatic conveying of large particles, but did not consider the influence of coal particle shape. Shibo Kuang et al. [36] proposed a CFD-DEM model considering the effect of air compressibility, which can be used to simulate large-scale delivery systems. The effectiveness of the model was verified by comparing the predicted pressure drop and the measured pressure drop of the dilute phase delivery system under different solid and gas flow rates.

Although many scholars have done research on pneumatic conveying devices, factors such as manufacturing and processing, site layout, and service life of the device should be considered in practical application. Therefore, this paper takes a company as the background to study the pneumatic conveying equipment of a large breeding enterprises, based on the economics of pneumatic conveying, in the horizontal pipeline when the conveying is stable. The four factors of the conveying wind speed, particle mass flow rate, pipe diameter, and particle size are studied on the velocity distribution of the particle in the horizontal pipe, the dynamic pressure change in the pipe, the pressure drop in the pipe, the solid mass concentration, and other pneumatic conveying characteristics, so as to ensure the maximum economic realization while meeting the conveying requirements, and the paper provides theoretical guidance for the company to build pneumatic conveying equipment.

2. Mathematical Model

2.1. Particle Suspension Velocity

Particles can be transported by air only when they meet a certain airflow velocity, that is, suspension velocity [37–39]. However, in a horizontal pipeline, particles are easy to be deposited at the lower part of the pipeline under the action of gravity, so in horizontal pneumatic conveying, the airflow velocity is generally greater than the suspension velocity. There are a variety of calculation formulas for suspension velocity in pneumatic conveying, the most widely used of which is the partitioned suspension velocity formula and its applicable particle size method, which is as follows:

1. Stokes zone

$$u_b = \frac{d_b^2(\rho_b - \rho_a)g}{18\mu} \quad (1)$$

$$\text{and } d_b \leq 1.225 \left[\frac{\mu^2}{\rho_b(\rho_b - \rho_a)} \right]^{\frac{1}{3}}$$

2. Allen zone

$$u_b = 1.195d_b \left[\frac{(\rho_b - \rho_a)^2}{\rho_a\mu} \right]^{\frac{1}{3}} \quad (2)$$

$$\text{and } 2.2 \left[\frac{\mu^2}{\rho_a(\rho_b - \rho_a)} \right]^{\frac{1}{3}} \leq d_b \leq 20.4 \left[\frac{\mu^2}{\rho(\rho_b - \rho_a)} \right]^{\frac{1}{3}}$$

3. Newton zone

$$u_b = 5.45 \sqrt{\frac{d_b(\rho_b - \rho_a)}{\rho_a}} \quad (3)$$

$$\text{and } 20.4 \left[\frac{\mu^2}{\rho_a(\rho_b - \rho_a)} \right]^{\frac{1}{3}} \leq d_b \leq 1100 \left[\frac{\mu^2}{\rho_a(\rho_b - \rho_a)} \right]^{\frac{1}{3}}$$

Where: u_b is the airflow velocity when the particles are suspended, m/s; ρ_a is air density; ρ_b is particle density; d_b is particle size; μ is the aerodynamic viscosity.

The suspension velocity is calculated as 10.8 m/s. In the actual conveying process, due to the energy loss caused by collision and friction, as well as the air flow nonuniformity in the pipeline, the actual conveying wind speed is generally 1.5–3.0 times of the particle

suspension velocity [40]. Therefore, considering the reliability of the test device, the actual air velocity used in this study is 18 m/s, 22 m/s, 26 m/s, and 30 m/s.

2.2. Gas Phase Control Equation

Gas phase is a continuous phase, considering the mass and momentum transfer between phases, and its motion law is controlled by the Navier–Stokes (N-S) equation [41–43]. Among them

Gas phase continuity equation:

$$\frac{\partial \varepsilon_a \rho_a}{\partial t} + \nabla \bullet (\varepsilon_a \rho_a v_a) = 0 \quad (4)$$

Gas phase momentum conservation equation:

$$\frac{\partial \varepsilon_a \rho_a v_a}{\partial t} + \nabla \bullet (\varepsilon_a \rho_a \mu_a v_a) = -\varepsilon_a \nabla p + \nabla \bullet (\varepsilon_a \mu_a \nabla v_a) + \varepsilon_a \rho_a g - F \quad (5)$$

where: ρ_a is fluid density; t is the time; v_a is the fluid velocity; ε_a is the volume fraction; μ_a is aerodynamic viscosity; p is fluid pressure; g is the acceleration of gravity, which is 9.81 m/s²; F is the volumetric force between particles and the fluid; and

$$F = \frac{\sum_{i=1}^n F_{D,i}}{V} \quad (6)$$

where: V is the volume of the computational cell.

2.3. Solid Phase Control Equation

As a solid phase in a two-phase flow, the motion of particles satisfies Newton's second law, and when solved in EDEM, its motion state can be decomposed into translation and rotation. The expressions of the two motion modes are:

Translational control equation:

$$m_i \frac{dv_{b,i}}{dt} = \sum_{j=1}^{k_i} F_{ij} + m_i g \quad (7)$$

rotation the control equation:

$$I_i \frac{dw_{p,i}}{dt} = \sum_{j=1}^{k_i} T_{ij} \quad (8)$$

where: $v_{b,i}$ is the particle translational velocity; F_{ij} is the interaction force between the particle and the fluid; m_i is the particle mass; I_i is the moment of inertia of the particle; $w_{p,i}$ is the particle angular velocity; T_{ij} is the particle torque.

3. Numerical Simulation Mode

After market research, it was found that the feed was particle, and the pig feed that was sold better was shaped like a two-bottom uneven cylinder, as shown in Figure 1. In this paper, particles with the largest number of four particle sizes were selected for modeling. In order to make the shape of the discrete element model more similar to that of feed particles and improve the simulation speed and effectiveness, this paper selected the tool of *Particle* for modeling in EDEM and used four spherules with equal diameter to stack into a discrete element model of feed, as shown in Figure 2.

According to the data of about 85 mm pipe diameter provided by the cooperative company, we selected 80 mm, 85 mm, 90 mm, and 95 mm internal diameter pipes to study the influence of pipe diameter on conveying characteristics. After creating the pipeline model, we first meshed the pipeline using ICEM software v 17.0. Among them, O-type

segmentation is adopted in ICEM, and the grid type is hexahedral unstructured mesh, the wall surface is encrypted to different degrees, then the mesh is output. We verified the grid independence and obtained the most appropriate number of grids under the four pipe diameters. Figure 3 shows the grid division results with a pipe diameter of 85 mm, a-a is the cross section of the grid, and b-b is a subsection of the sampling section.

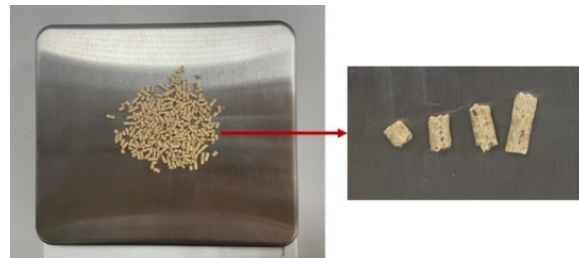


Figure 1. Particle feed morphology.



Figure 2. Discrete element model of particle feed.

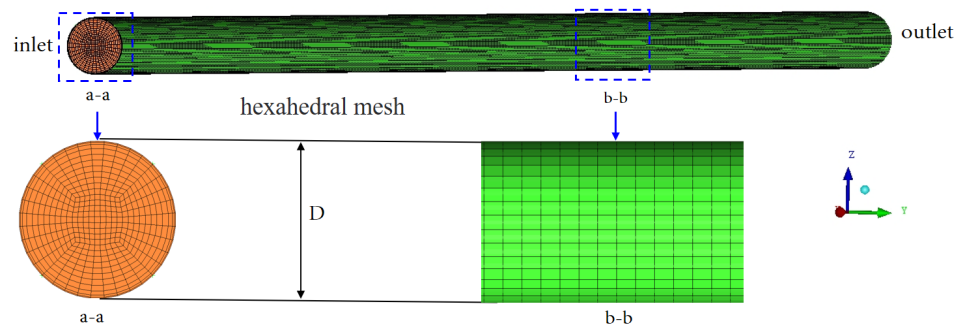


Figure 3. Horizontal pipe meshing.

3.1. Pipe and Particle Parameters

In order to make the test results of the subsequent test bench easy to observe, the pipeline material selects acrylic plates with good transparency, strong insulation, and high recovery rate, whose density, Poisson’s ratio, and shear modulus are 1200 kg/m^3 , 0.4, and $1.07 \times 10^9 \text{ Pa}$, respectively. Particle parameters were calibrated according to the injection cross section method of Peng Fei et al. [44], as shown in Table 1.

Table 1. Pipe and particle parameters.

Parameters	Pipeline	Particle
Density (kg/m^3)	1200	800
Poisson’s ratio	0.4	0.4
shear modulus (Pa)	1.07×10^9	3.93×10^7
coefficient of collision restitution	0.5	0.53
coefficient of static friction	0.5	0.41
coefficient of rolling friction	0.01	0.08

3.2. Benchmark Working Conditions and Simulation Parameter Settings

In order to study the influence of different factors on pneumatic conveying characteristics, the benchmark working conditions parameters established as follows: the conveying wind speed is 22 m/s, the particle mass flow rate is 0.2 kg/s, the pipe diameter is 85 mm, and the particle size is 3 mm. The simulation grouping and parameters settings are shown in Table 2.

Table 2. Simulation grouping and parameters settings.

	Conveying Wind Speed (m/s)	Particle Mass Flow Rate (kg/m ³)	Pipe Diameter (mm)	Particle Size (mm)
1	18	0.2	85	3
2	22	0.2	85	3
3	26	0.2	85	3
4	30	0.2	85	3
5	22	0.4	85	3
6	22	0.6	85	3
7	22	0.8	85	3
8	22	0.2	80	3
9	22	0.2	90	3
10	22	0.2	95	3
11	22	0.2	85	2
12	22	0.2	85	4
13	22	0.2	85	5

Firstly, the simulation results under the benchmark working condition were analyzed to obtain the general rules. Then, the control variable method was used to simulate and analyze different influencing factors, and the influence of conveying wind speed, particle mass flow, pipe diameter, particle size, and other factors on the pneumatic conveying characteristics was studied.

3.3. Simulation Parameter Settings

The simulation was solved by CFD-DEM coupling. In EDEM, firstly, we import the mesh into EDEM, then create particles, set parameter of particles and pipes according to Table 1. Next, add the contact parameters between particles and particles and between particles and pipes, and set the size of the parameters according to Table 1. At the same time, a particle factory was created 0.2 m away from the inlet in "Geometries", and mass flow rate of particles was set according to the simulation requirements. The particle contact model was Hertz–Mindlin (no slip) with RVD Rolling Friction, and the particle–pipeline contact model was Hertz–Mindlin with Archard Wear. The direction of gravity acceleration is set to the negative Z-axis, the size is 9.81 m/s². Finally, the Rayleigh time step is set to 3×10^{-6} , and the Cell size is set to 5R.

In Fluent, firstly, we choose 3D double precision for the solver. After, we import the mesh and check, select the pressure base, transient solution, and set the gravitational acceleration to the negative Z-axis, with the size of 9.81 m/s². Then, connected with EDEM, the solution selection is set as follows:

Models: The model adopts the standard k-ε turbulence model;

Boundary Conditions: Inlet choose the velocity inlet, outlet choose the pressure outlet, hydraulic diameter is set as the size of the actual pipe diameter;

Solution Methods: Choose the SIMPLEC algorithm;

Solution Initialization: Choose the Standard Initialization, and initialize from the inlet;

Finally, we set the time step to 3×10^{-4} and the number of time steps is 12,000.

The simulation parameters as shown in Figure 4.

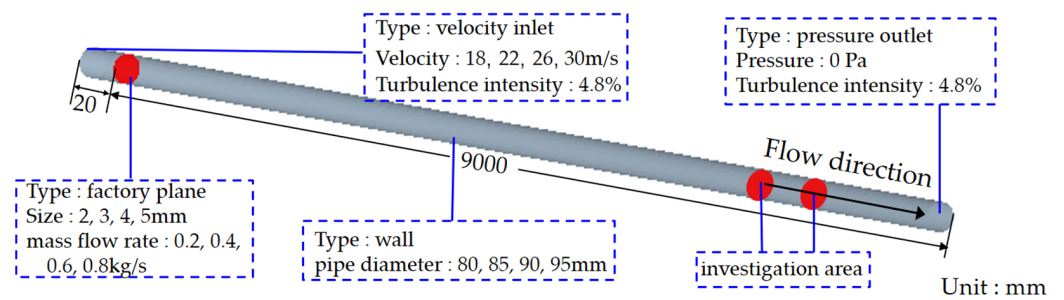


Figure 4. Simulation model parameters.

4. Simulation Results and Analysis

The benchmark working conditions were simulated, and the simulation results show that after entering the pipeline, the particles accelerate forward under the drag force provided by the wind. At the same time, the particles settle down under the action of gravity until they collide with the pipe wall. After obtaining enough momentum, the particles begin to suspend in the pipeline. When the motion reaches dynamic stability, more particles are deposited at the bottom of the pipeline, and the closer to the upper part of the pipe, the fewer the particles, the more obvious the suspension phenomenon.

In the dynamic stability stage of suspension movement, a pipe with a length of 0.5 m at a distance of 7.5–8 m from the inlet was intercepted for analysis. In the process of conveying, the particle velocities at different positions vary greatly, so this paper divides the interception section into three zones: low-speed zone, transition zone, and high-speed zone according to the particle velocity, as shown in Figure 5. The experimental results show that from the high-speed zone to the transition zone to the low-speed zone, the number of particles increases, and the solid phase concentration per unit volume increases. Meanwhile, the collisions between particles and between particles and walls increase, leading to the increase of energy loss. At the same time, the porosity decreases, which leads to the decrease of particle acceleration space and therefore particle velocity decreases.

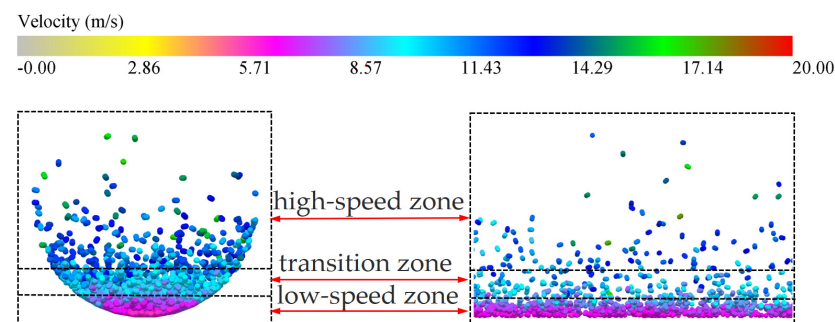


Figure 5. Horizontal cross-sectional partition cloud diagram.

4.1. Simulation Results and Analysis of Different Conveying Wind Speeds

In order to study the influence of conveying wind speed on the conveying characteristics of particles, the conveying wind speed of other working conditions is set to 18 m/s, 26 m/s, and 30 m/s based on the benchmark working conditions, and the control variable method is used for simulation analysis. The simulation results are as follows. Figure 6a is the fluid dynamic pressure cloud diagram under different conveying wind speeds in the sampling section. It can be seen from (a) that, with the increase of conveying wind speed, the maximum dynamic pressure in the pipe increases from 300 Pa to 758 Pa, and the minimum from 29 Pa to 274 Pa, showing an overall increasing trend. Figure 6b shows the cloud diagram of particle mass concentration changes under different conveying wind speeds in the sampling section. It can be seen from (b) that, with the increase of conveying wind speed, the particle mass concentration in the pipe presents a decreasing trend, and the

maximum dynamic pressure and minimum mass concentration appear in the high-speed zone, while the minimum dynamic pressure and maximum mass concentration appear in the low-speed zone.

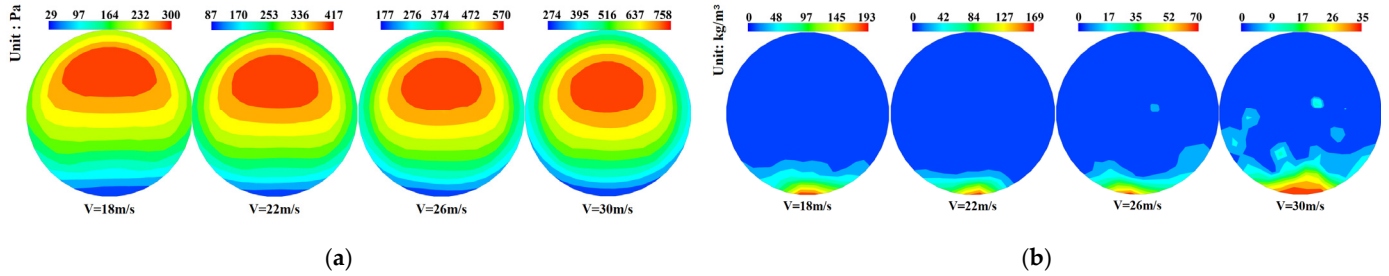


Figure 6. Distribution cloud diagram of fluid dynamic pressure and solid mass concentration under different conveying wind speeds. (a) Fluid dynamic pressure cloud diagram, Pa; (b) particle mass concentration cloud diagram, kg/m^3 .

When the conveying wind speed increases, the dynamic pressure increases and the particle mass concentration decreases. The analysis shows that, when the dynamic pressure increases, the kinetic energy of the particles increases, and the particles will be transported out faster in the pipeline. Meanwhile, the number of particles in the pipeline of the same length decreases, so the particle mass concentration decreases. At this time, the porosity of particles increases, which means that the interval between particles increases, and the probability of particle collision decreases. In actual transportation, collision will lead to breakage, and the breakage of particles reduced by collision will also be reduced. That is, the number of complete particles transported will increase, and the transportation efficiency will increase, which is conducive to the economy of transportation.

Figure 7 shows the relationship between the average velocity of particles in the 0.5 m pipe length in the three zones with time under different conveying wind speeds. It can be seen from Figure 7 that the final stable velocity of particle groups in the three zones differs significantly with the change of conveying wind speed. The larger the conveying wind speed, the sooner the particles arrive at the sampling section, and the smaller the conveying wind speed, the later the time for particles to reach dynamic equilibrium in the sampling section, which is in line with the actual conditions.

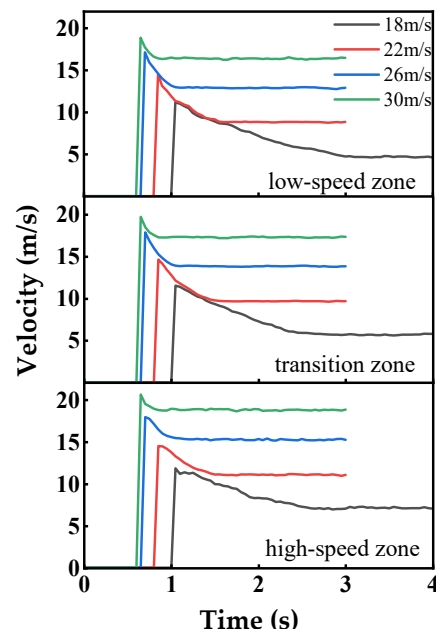


Figure 7. Variation of average particle velocity with time under different conveying wind speeds.

Figure 8a shows the average value of the final stable velocity of the particles in the three zones with the change of the conveying wind speed. From (a), we see that with the increase of conveying wind speed, the average velocity of the particle group after stabilization increases approximately linearly, and the value of the average velocity changes greatly. The trend of change is consistent in the three zones. Figure 8b shows the pressure drop of fluid along the pipe under different conveying wind speeds in the sampling section 7.5 m to 8 m away from the inlet. As can be seen from (b), the pressure drop gradually increases with the increase of conveying wind speed, but when the wind speed increases from 18 m/s to 22 m/s, the pressure drop increase rate is small. The pressure drop in gas-solid two-phase flow refers to the size of the driving force being consumed. In this paper, the significance is generally speaking the quantity of transported particles. The higher the mass concentration of particles in the pipe, the fewer particles are transported out and the smaller the pressure drop. Therefore, the pressure drop is changing because when the conveying wind speed is 18 m/s and 22 m/s, the particle mass concentration is large, and the difference is small, and when the conveying wind speed is 26 m/s and 30 m/s, the particle mass concentration is significantly reduced, and the difference is large compared with the previous two working conditions, so there will be a large difference in the change rate of pressure drop. At the same time, when there are more particles in the pipe, the porosity between particles is small, which will lead to the increase of particle collision and energy loss. Therefore, the economic wind speed of this group of simulation is 30 m/s.

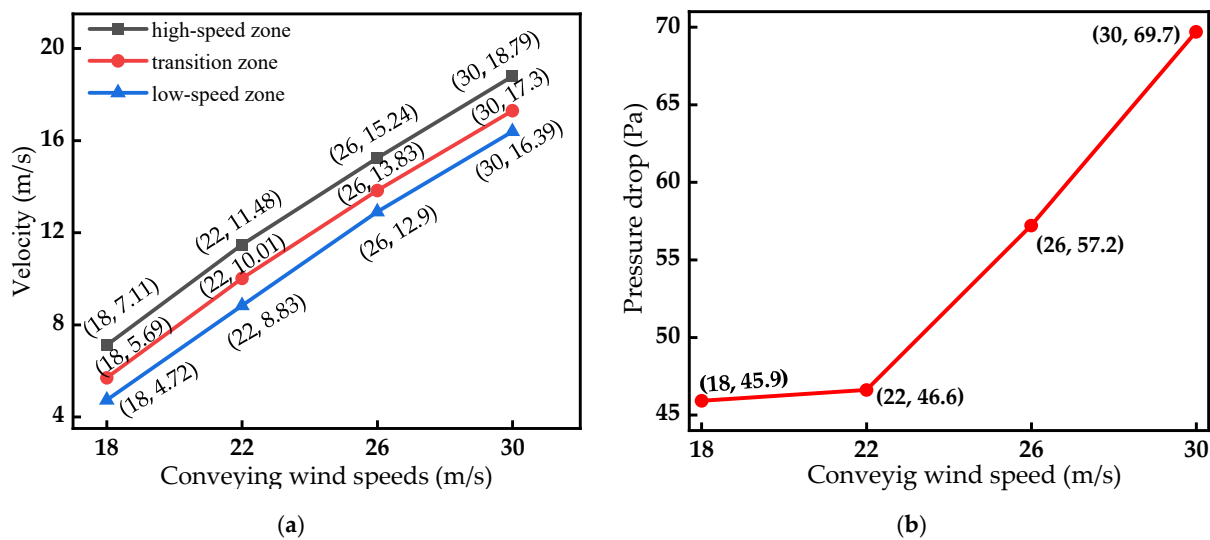


Figure 8. Velocity and pressure drop change curve with conveying wind speed. (a) Variation of average value of final stable velocity with conveying wind speed; (b) Variation of pipe pressure drop with conveying wind speed.

Therefore, in actual production, within the range allowed by calculation, the selection of wind speed should consider the collision, pressure drop, conveying efficiency, and other factors. The simulation results show that the conveying effect is better when the conveying wind speed is three times the calculated value based on the theoretical suspension velocity. That is, when $G_s = 0.2$ kg/s, $d = 3$ mm, and $D = 85$ mm, the conveying effect is ideal when $V = 30$ m/s is selected.

4.2. Simulation Results and Analysis of Different Mass Flow Rates

In order to study the influence of mass flow rate on the conveying characteristics of particles, the mass flow rate of other working conditions is set to 0.4 kg/s, 0.6 kg/s, or 0.8 kg/s based on the benchmark working conditions, and the control variable method is used for simulation analysis. The simulation results are as follows. Figure 9a is the fluid

dynamic pressure cloud diagram under different mass flow rates in the sampling section. Figure 9b shows the cloud diagram of particle mass concentration changes under different mass flow rates in the sampling section. It can be seen from Figure 9 that the overall dynamic pressure in the pipe does not change much with the increase of particle mass flow rate. From the specific value, the maximum value of dynamic pressure in the pipe increases, while the minimum value decreases, showing different changing trends. The increase of particle mass flow rate means that the number of particles in the pipeline increases. However, the conveying wind speed is unchanged, that is, the total energy transferred to the particles by the wind is unchanged. When the number of particles increases, the energy obtained by each particle will decrease, and the dynamic pressure is small, resulting in a small particle velocity. The number of particles suspended in the high-speed zone is little, the kinetic energy of each particle is larger, and the dynamic pressure is larger.

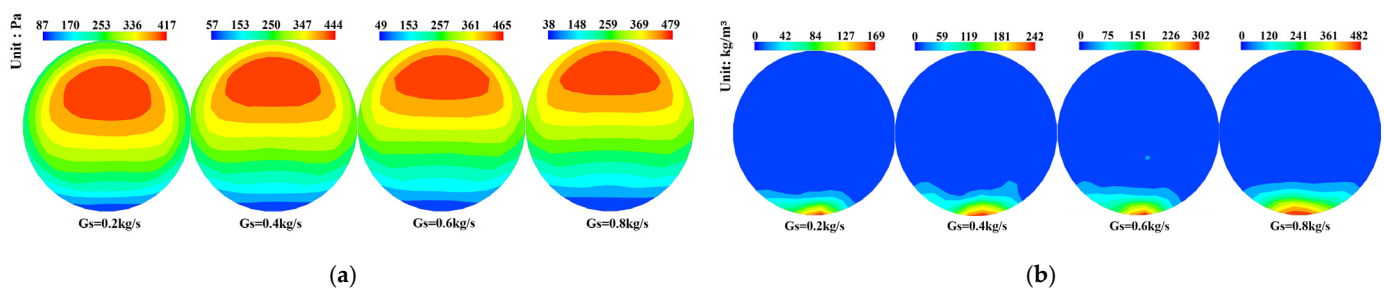


Figure 9. Distribution cloud diagram of fluid dynamic pressure and solid mass concentration under different mass flow rates. (a) Fluid dynamic pressure cloud diagram, Pa; (b) particle mass concentration cloud diagram, kg/m^3 .

As can be clearly seen from the picture, with the increase of particle mass flow rate, the particle mass concentration in the pipeline also increases, which is in line with the actual situation. From the perspective of the low-speed zone, when the particle mass flow rate increases at the rate of 0.2 kg/s , the increment of particle mass concentration is 73, 60, and 180 respectively, that is, when the particle mass flow rate increases from 0.6 kg/s to 0.8 kg/s , the particle mass concentration changes the most, at this time, the porosity of particles is small, and the collision between particles increases, and it will lead to the increase of breakage in actual transportation.

Figure 10 shows the relationship between the average velocity of particles in the 0.5 m pipes length in the three zones with time under different mass flow rates. It can be seen from Figure 10 that under the condition of a certain conveying wind speed, the increase of particle mass flow rate has almost no effect on the time for the first particle to arrive at the sampling section, but has an impact on the time for the particle group to reach stability in the 0.5 m long sampling section, that is, the greater the particle mass flow rate, the longer the time for dynamic equilibrium. It can also be seen from the figure that the influence of particle mass flow rate on the average velocity of particle groups in the high-speed zone is lower than that in the low-speed zone.

Figure 11a shows the average value of the final stable velocity of the particles in the three zones with the change of the mass flow rates, it can be seen from Figure 11a that in the stability of the conveying stage, with the increase of particle mass flow rate, the average stable speed in the high-speed zone decreases by 1.56 , the transition zone decreases by 2.62 , and the low-speed zone decreases by 2.97 . The overall changes are small, but the change in the high-speed region is the smallest, indicating that the mass flow rate has a greater impact on the low-speed zone when other conditions remain unchanged.

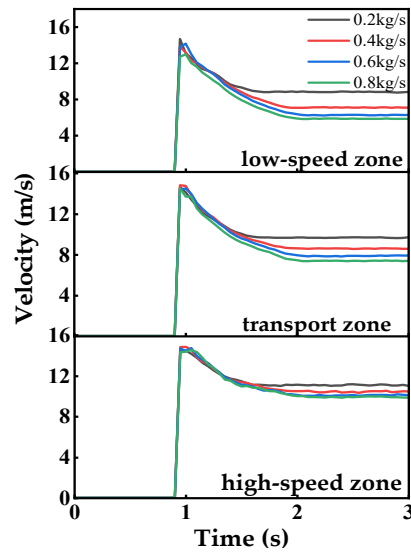


Figure 10. Variation of average particle velocity with time under different mass flow rate.

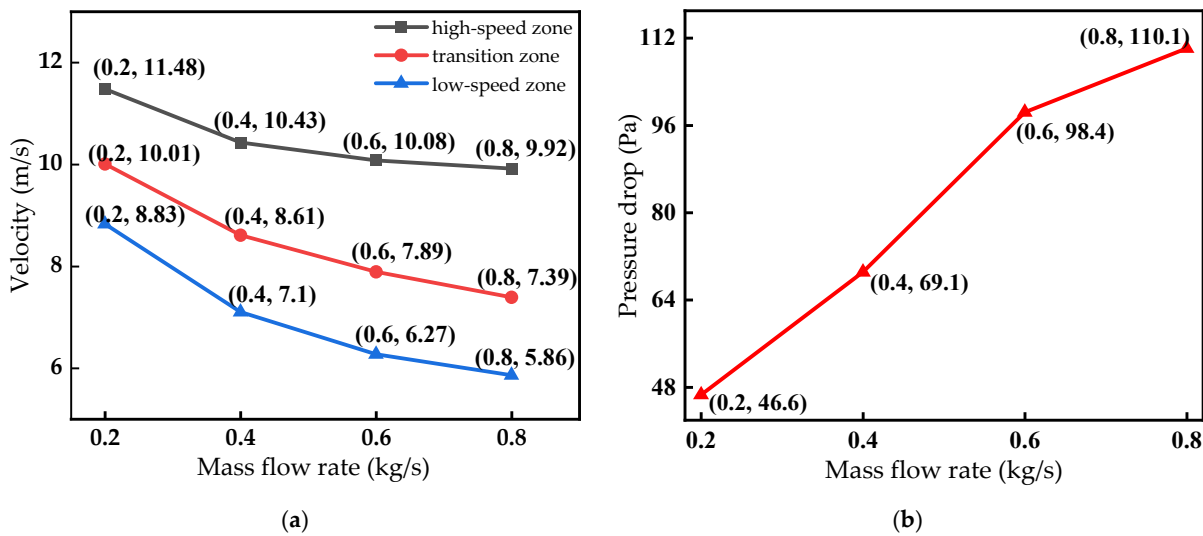


Figure 11. Velocity and pressure drop change curve with mass flow rate. (a) Variation of average value of final stable velocity with mass flow rate; (b) Variation of pipe pressure drop with mass flow rate.

Figure 11b shows the pressure drop of fluid along the pipe under different mass flow rates in the sampling section 7.5 m to 8 m away from the inlet. From Figure 11b, it can be seen that with the increase of mass flow rate, the pressure drops in the 0.5 m long pipeline and increases gradually. Specifically, when the particle mass flow rate is 0.2–0.6 kg/s, the pressure drop increases roughly linearly, and when the particle mass flow rate increases from 0.6 kg/s to 0.8 kg/s, the increase range of pressure drop decreases. From the analysis of the particle mass concentration in the pipe, it can be seen that when the particle mass flow rate increases from 0.6 kg/s to 0.8 kg/s in the low-speed zone, the particle mass concentration increment is 180, indicating that the particle retention time in the pipe becomes longer, and the time used to completely transport the particle out of the pipe increases. The amount of particles output per unit time increases less than when the mass flow rate is 0.6 kg/s, and the pressure drop increases less. More pressure drop indicates that there are many losses in the conveying process. However, when the particle mass flow rate increases from 0.6 kg/s to 0.8 kg/s, the increase rate of pressure drops decreases. In other words, when the particle throughput increases, the increment

of pressure drops decreases, indicating the economic mass flow rate of 0.8 kg/s under the working conditions of this group.

This study is for thin phase pneumatic conveying, and the particle mass flow rate is small. From the simulation results, the larger the mass flow rate, the better the conveying effect. However, in the actual transportation, when the particle mass flow rate is too large and the wind speed is unchanged, the particles will be blocked due to the failure to send out in time. Therefore, in the actual production, the particle mass flow rate should be set with a larger value according to the demand of the enterprise on the premise of not causing accumulation and blockage. This group of simulations shows that when $V = 22$ m/s, $d = 3$ mm, and $D = 85$ mm, the conveying effect is better when $G_s = 0.8$ kg/s.

4.3. Simulation Results and Analysis of Different Pipe Diameters

In order to study the influence of pipe diameter on the conveying characteristics of particles, the pipe diameter of other working conditions is set to 80 mm, 90 mm, or 95 mm based on the benchmark working conditions, and the control variable method is used for simulation analysis. The simulation results are as follows. Figure 12a is the fluid dynamic pressure cloud diagram under different pipe diameters in the sampling section. Figure 12b shows the cloud diagram of particle mass concentration changes under different pipe diameters in the sampling section. It can be seen from Figure 12 that when other conditions remain unchanged and pipe diameter increases by 5 mm, the numerical variation of dynamic pressure and particle mass concentration in the pipe is small, and the solid phase mass concentration distribution is slightly different. It shows that when the diameter of the pipe is changed in a small range under the condition that conveying wind speed, mass flow rate, and pipe diameter are unchanged, the impact on the motion state of the particles is small.

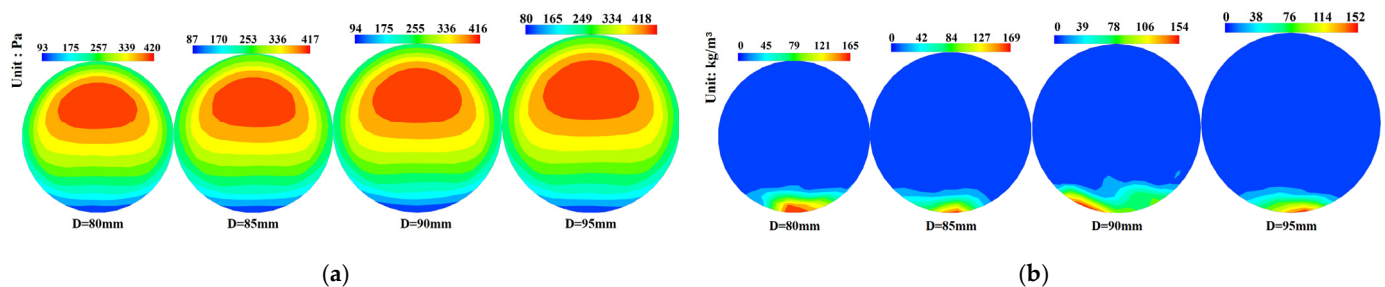


Figure 12. Distribution cloud diagram of fluid dynamic pressure and solid mass concentration under different pipe diameters. (a) Fluid dynamic pressure cloud diagram, Pa; (b) particle mass concentration cloud diagram, kg/m³.

Figure 13 shows the relationship between the average velocity of particles in the 0.5 m pipes length in the three zones with time under different pipe diameters. It can be seen from Figure 13, the average velocity of particles in the three zones within different pipe diameters is not very different, and the time of first arriving at the sampling section is irregular. From the point of view of the average velocity after stable conveying, the change of pipe diameter in a small range has little influence on the average velocity of conveying particles in each region. On the local magnified view after the convey is stabilized, we can see that the speed changes with time in the high-speed zone are more severe than in the transition zone and the low-speed zone.

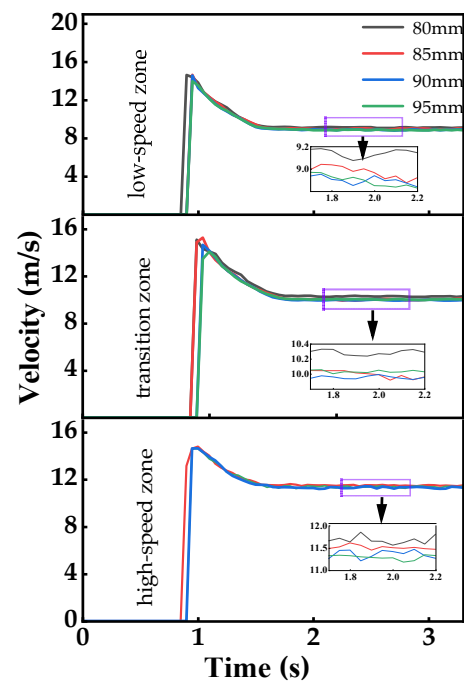


Figure 13. Variation of average particle velocity with time under different pipe diameters.

Figure 14a shows the average value of the final stable velocity of the particles in the three zones with the change of the pipe diameters, Figure 14b shows the pressure drop of fluid along the pipe under different pipe diameters in the sampling section 7.5 m to 8 m away from the inlet. From the specific value of Figure 14a, with the increase of pipe diameter, the average velocity in the high-speed zone decreases with a small value, and the average velocity of particles in the transition zone and the low-speed zone is the smallest when the pipe diameter is 90 mm, showing different changing trends. From Figure 14b, in the 0.5 m long pipe, when the conveying wind speed is 22 m/s and the particle mass flow rate is 0.2 kg/s, the pressure drop in the pipe gradually decreases with the increase of the pipe diameter. The pressure drop decreases linearly when the pipe diameter increases from 80 mm to 90 mm, and the pressure drop decreases becomes smaller when the pipe diameter increases from 90 mm to 95 mm. Pressure loss in gas-solid two-phase flow includes accelerated pressure loss, frictional pressure loss, gravitational compression, and local pressure loss. The analysis of the changes of pressure loss in different pipe diameters shows that when the pipe diameter increases from 80 mm to 90 mm, the average velocity of particles in the pipe gradually decreases, which means that acceleration decreases with the increase of pipe diameter, so accelerated pressure loss decreases. When the pipe diameter increases from 90 mm to 95 mm, the average velocity of particles in the low-speed zone and transition zone increases slightly, while the average velocity of particles in the high-speed zone decreases. Therefore, when the pipe diameter increases from 90 mm to 95 mm, the accelerated pressure loss is less than that in the previous working condition. Under the condition of constant wind speed, with the increase of pipe diameter, the flow of wind in the pipe increases. In actual production, larger pipe diameter requires the use of more powerful fans, so the actual power consumption will also increase. From the analysis of pressure drop, when the pipe diameter increases, the pressure drop does not decrease much. At the same time, large diameter pipe will also consume more raw material. Therefore, considering the actual power consumption and the raw materials for the pipes, the economic diameter of this group of working conditions is 80 mm.

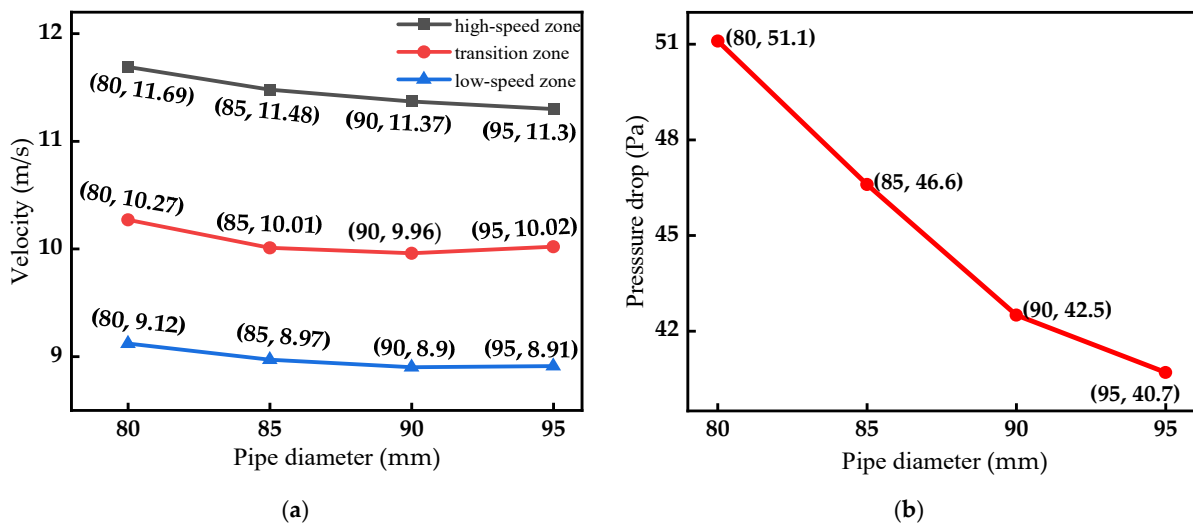


Figure 14. Velocity and pressure drop change curve with pipe diameter. (a) Variation of average value of final stable velocity with pipe diameter; (b) variation of pipe pressure drop with pipe diameter.

Therefore, in actual production, because pipe diameter has little influence on particle velocity and pipe pressure drop, taking into account power consumption in actual production and pipe consumables, pipe diameter should be set to a small value. This group of simulations shows that when $V = 22 \text{ m/s}$, $G_s = 0.2 \text{ kg/s}$, and $d = 3 \text{ mm}$, the conveying effect is more ideal when $D = 80 \text{ mm}$.

4.4. Simulation Results and Analysis of Different Particle Sizes

In order to study the influence of particle size on the conveying characteristics of particles, the particle size of other working conditions is set to 2 mm, 4 mm, or 5 mm based on the benchmark working conditions, and the control variable method is used for simulation analysis. The simulation results are as follows. Figure 15a is the fluid dynamic pressure cloud diagram under different particle sizes in the sampling section. Figure 15b shows the cloud diagram of particle mass concentration changes under different particle sizes in the sampling section.

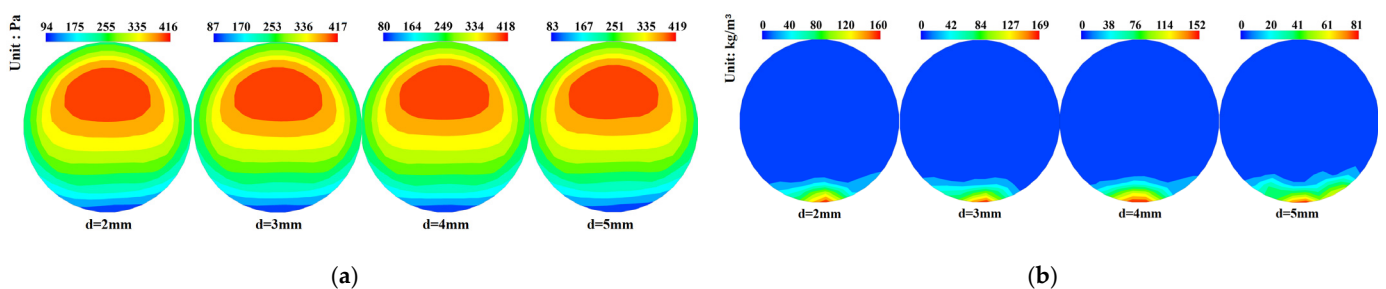


Figure 15. Distribution cloud diagram of fluid dynamic pressure and solid mass concentration under different particle sizes. (a) Fluid dynamic pressure cloud diagram, Pa; (b) particle mass concentration cloud diagram, kg/m^3 .

It can be seen from Figure 15 that the dynamic pressure of the fluid in the three zones has little change under different particle sizes, while the mass concentration of the particles in the low-speed zone changes significantly when the particle size increases from 4 mm to 5 mm. When the mass flow rate of particles is the same, the change of particle size will affect the number of particles. If the mass flow rate is the same, the total mass of different particle sizes in unit time is the same. Under the condition of constant density, the larger the particle size, the larger the mass of a single particle, so the total number of

particles will be reduced. In Figure 15a, the dynamic pressure of particles with different particle sizes changes little, indicating that the total energy obtained by particles has little difference, that is, the average velocity difference of particle groups is small. In Figure 15b, the abrupt change of particle mass concentration in the low-speed region indicates that the total mass of particles with 5 mm diameter is more than that of particles transported out of the pipeline in the same time.

Figure 16 shows the relationship between the average velocity of particles in the 0.5 m pipes length in the three zones with time under different particle sizes. As can be seen from Figure 16, the first time for particles of different sizes to reach the sampling segment varies slightly in the three zones. The first arrival time of particles with different sizes in the low-speed zone is almost the same, while the time when the high-speed zone and the transition zone first reach the sampling section is significantly different than that in the low-speed zone. In addition, the average velocity of 2 mm particle group in the sampling section reaches dynamic equilibrium first.

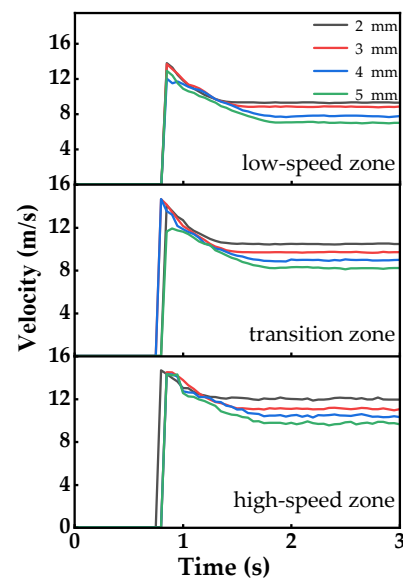


Figure 16. Variation of average particle velocity with time under different particle sizes.

Figure 17a shows the average value of the final stable velocity of the particles in the three zones with the change of the particle sizes, Figure 17b shows the pressure drop of fluid along the pipe under different particle sizes in the sampling section 7.5 m to 8 m away from the inlet. It can be seen from Figure 17a that the average velocity of particle groups in the three zones decreases approximately linearly with the increase of particle size, and the change trend is consistent. The decreases in the three zones are 2.26, 2.23, and 2.28 respectively. It can be seen from Figure 17b that the pressure drops inside the 0.5 m length pipe gradually increases with the increase of particle size, and the pressure drop increases by 0.8, 0.5, and 1.2, respectively. The pressure drop increases the most when the particle size increases from 4 mm to 5 mm. From the analysis of particle mass concentration, when the particle size increases from 4 mm to 5 mm, the mass concentration of particles in the low-speed zone changes greatly, indicating that there is a large difference in the quantity of particles in the conveying pipe, so the pressure drop is large. From the analysis of particle size, the larger the particle size, the greater the loss caused by the collision, the more energy the wind pressure is used to compensate for the collision, and the pressure drop in the pipeline will increase.

Generally speaking, when the particle size increases, the average velocity of the particle group decreases in the three zones, and the pressure drop gradually increases. However, the specific numerical changes are not significant, that is, under the condition of a certain conveying wind speed, mass flow rate, and pipe diameter, the change of particle size in

a small range has little influence on the conveying characteristics. From the suspension velocity formula, the larger the particle size is, the larger the wind speed required for suspension motion is. From Figure 17a, when the particle size increases from 2 mm to 3 mm, the stability velocity of the particle group decreases less. Therefore, in order to achieve good fluidity, the velocity should not be too small, so the particle size of 3 mm under this group of working conditions is the economic particle size.

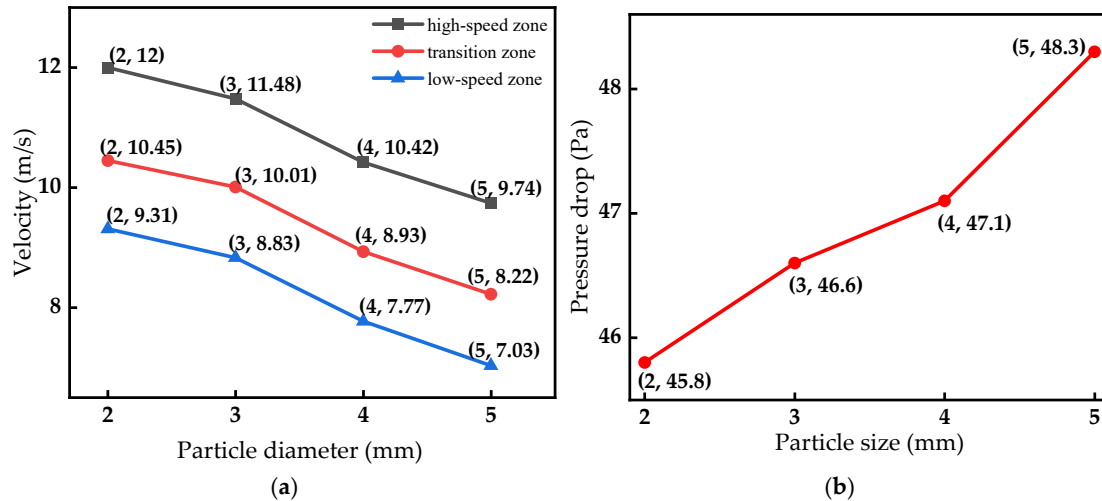


Figure 17. Velocity and pressure drop change curve with pipe diameter. (a) Variation of average value of final stable velocity with particle size; (b) variation of pipe pressure drop with particle size.

Therefore, in the actual production, when transporting large particle materials, it is necessary to provide greater wind speed. This group of simulations shows that when $V = 22$ m/s, $G_s = 0.2$ kg/s, and $D = 85$ mm, the conveying effect is better when $d = 3$ mm.

5. Conclusions

In this paper, through the analysis of the simulation experimental results, the influence of different factors on the conveying characteristics is obtained, which is as follows:

1. The conveying wind speed has the greatest influence on pneumatic conveying. With the increase of conveying wind speed, the dynamic pressure increases, while the mass concentration of particles decreases. The final stable velocity of the particle group in the three zones increases linearly with the increase of the conveying wind speed, and the greater the wind speed, the shorter the time for the particles to reach the dynamic stability. The pressure drops in the pipe also increased with the increase of the conveying wind speed, but the change rate of pressure drop was small when the conveying wind speed increased from 18 m/s to 22 m/s. In actual production, the greater the wind speed, the greater the required fan power and the more power consumption, so the selection of wind speed should be a comprehensive consideration of collision, pressure drop, transport efficiency and other factors.
2. Particle mass flow rate has great influence on mass concentration. With the increase of particle mass flow rate, the maximum value of dynamic pressure increases and the minimum value decreases, showing different changing trends, and the particle mass concentration increases obviously. With the increase of the mass flow rate, the final stable velocity of the particle group in the three zones decreases, and the smaller the mass flow rate, the shorter the time for the particle group to reach the dynamic stability. The pressure drops also increased with the increase of mass flow rate, but when the mass flow rate of particles increased from 0.6 kg/s to 0.8 kg/s, the increase of pressure drop decreased. In the actual production, when the particle mass flow rate is too large and the wind speed is unchanged, the particles will be blocked due to

- the failure to send out in time. In this paper, it is thin phase transportation, and no blockage occurs.
3. Pipe diameter has little effect on conveying characteristics. When the pipe diameter is changed in a small range, the dynamic pressure in the tube and the mass concentration of the particles have little effect. The final stable velocity of the particle group in the high-speed zone decreases with the increase of the diameter of the pipe, while the transition zone and the low-speed zone first decrease and then increase. Generally speaking, the velocity values change little. The pressure drops decrease with the increase of pipe diameter. In actual production, the pipe diameter has little influence on particle movement, so the selection of pipe diameter should refer to the pipeline consumables and the power of the fan.
 4. Particle size has some influence on pneumatic conveying. With the increase of particle size, the change of dynamic pressure is not obvious, and the particle mass concentration changes greatly when the particle size increases from 4 mm to 5 mm. The final stable velocity of particle groups in the three zones decreases with the increase of particle size. The pressure drop increases with the increase of particle size, and when the particle size increases from 4 mm to 5 mm, the pressure drop increases the most. In actual production, it is known from the suspension speed formula that a larger wind speed should be provided when transporting large-sized particle materials to ensure good fluidity of particles.

Author Contributions: Conceptualization, C.W. and W.L.; methodology, C.W. and B.L.; software, W.L. and S.J.; validation, C.W. and B.L.; investigation, C.W., W.L., and Z.J.; resources, C.W. and B.L.; data curation, C.W., W.L., and H.M.; writing—original draft preparation, W.L.; writing—review and editing, C.W., B.L., and Z.J.; visualization, W.L., S.J., and H.M.; project administration, C.W.; funding acquisition, B.L. All authors have read and agreed to the published version of the manuscript.

Funding: This research was funded by the National Natural Science Foundation of China (No. 21401168).

Institutional Review Board Statement: Not applicable.

Informed Consent Statement: Not applicable.

Data Availability Statement: The data presented in this study are available upon request from the corresponding author.

Conflicts of Interest: The authors declare no conflict of interest.

Nomenclature

V	Conveying wind speed, m/s
G_s	Mass flow rates, kg/s
D	Pipe diameters, mm
d	Particle size, mm
u_b	airflow velocity, m/s
ρ_a	air density, kg/m ³
ρ_b	particle density, kg/m ³
μ	aerodynamic viscosity
v_a	gas velocity, m/s
v_b	solid velocity, m/s
ε_a	volume concentration of the gas
ε_b	volume concentration of the solid
μ_a	effective viscosity of gas
μ_b	effective viscosity of solid
P	gas phase pressure
β	drag coefficient

References

1. Xie, B.; Huang, J.; Huang, C.; Wang, Y.; Shi, S.; Huang, L. Stable isotopic signatures ($\delta^{13}\text{C}$ and $\delta^{15}\text{N}$) of suspended particulate organic matter as indicators for fish cage culture pollution in Sansha Bay, China. *Aquaculture* **2020**, *522*, 735081. [[CrossRef](#)]
2. Gizachew, H.; Bereket, M.T.; Wubit, W.; Mishamo, S.; Teshale, S. Epidemiological investigation of morbidity and mortality of improved breeds of chickens in small holder poultry farms in selected districts of Sidama Region, Ethiopia. *Heliyon* **2022**, *8*, e10074.
3. Yogeve, U.; Vogler, M.; Huang, O.; Londong, J.; Gross, A. Phosphorous recovery from a novel recirculating aquaculture system followed by its sustainable reuse as a fertilizer. *Sci. Total Environ.* **2020**, *722*, 137949. [[CrossRef](#)] [[PubMed](#)]
4. Singh, G.; Deng, T.; Bradley, M.S.A.; Ellis, R. Advanced Assessment of Biomass Materials Degradation in Pneumatic Conveying Systems: Challenges and Applications. *Appl. Sci.* **2023**, *13*, 1960. [[CrossRef](#)]
5. Shijo, J.S.; Behera, N. Statistical analysis of fluidized dense phase conveying of fine particles. *Powder Technol.* **2022**, *404*, 117441.
6. Du, J.; Heng, Y.F.; Xia, J.F.; Hu, M.J.; Zou, G. Simulation of Non-Spherical Rice Seed Motion in Pneumatic Conveying with Bend by CFD-DEM: Original papers. *Int. J. Fluid Mach. Syst.* **2021**, *14*, 300–308. [[CrossRef](#)]
7. Dou, J.; Wang, K.Y.; Chen, J.Q.; Chen, D.G. Application and development of stop-pan feeding system in feed conveying link of large-scale pig farm. *J. Feed. Res.* **2022**, *45*, 134–138.
8. Ali, K.A.M.; Zong, W.; Md-Tahir, H.; Ma, L.; Yang, L. Design, Simulation and Experimentation of an Axial Flow Sunflower-Threshing Machine with an Attached Screw Conveyor. *Appl. Sci.* **2021**, *11*, 6312. [[CrossRef](#)]
9. Tian, Y.; Yuan, P.; Yang, F.; Gu, J.; Chen, M.; Tang, J.; Su, Y.; Ding, T.; Zhang, K.; Cheng, Q. Research on the Principle of a New Flexible Screw Conveyor and Its Power Consumption. *Appl. Sci.* **2018**, *8*, 1038. [[CrossRef](#)]
10. Othmer, D.F. *Fluidization*, 1st ed.; Reinhold Publishing Corporation: New York, NY, USA, 1956; pp. 9–21.
11. Marcus, R.; Leung, L.; Klinzing, G.; Rizk, F. Pneumatic Conveying of Solids: A Theoretical and Practical Approach. *Dry. Technol.* **1993**, *11*, 859–860. [[CrossRef](#)]
12. Mills, D. *Pneumatic Conveying Design Guide*; Elsevier Butterworth-Heinemann: Oxford, UK, 2015.
13. Reinauer, T.V. Hygienic and economic advantages of low pressure pneumatic conveying. *Am. Ind. Hyg. Assoc. Q.* **1957**, *18*, 59–64. [[CrossRef](#)] [[PubMed](#)]
14. An, L.; Liu, W.; Ji, Y.; Shen, G.; Zhang, S. Detection of Pneumatic Conveying by Acoustic Emissions. *Appl. Sci.* **2019**, *9*, 501. [[CrossRef](#)]
15. Zhu, R.; Luo, C.; Li, X.; Yan, F. Experimental Quantification of Local Pressure Loss at a 90° Bend in Low-Pressure Dilute-Phase Pneumatic Conveying of Coarse Particles. *Int. J. Chem. Eng.* **2019**, *2019*, 6454958. [[CrossRef](#)]
16. Beaulac, P.; Issa, M.; Ilinca, A.; Brousseau, J. Parameters Affecting Dust Collector Efficiency for Pneumatic Conveying: A Review. *Energies* **2022**, *15*, 916. [[CrossRef](#)]
17. Sharma, A.; Mallick, S.S. An investigation into pressure drops through bends in pneumatic conveying systems. *Part. Sci. Technol.* **2021**, *39*, 180–191. [[CrossRef](#)]
18. Tripathi, N.M.; Portnikov, D.; Levy, A.; Kalman, H. Bend pressure drop in horizontal and vertical dilute phase pneumatic conveying systems. *Chem. Eng. Sci.* **2019**, *209*, 115228. [[CrossRef](#)]
19. Oscar, P. Pressure Drops in the Pneumatic Conveyance of Solids. *J. Appl. Mech.* **1952**, *19*, 425–431.
20. Cornish, G.K.; Charity, L.F. Pressure Drop in Elbows of a Pneumatic Conveying System. *Trans. ASAE* **1966**, *9*, 29–0031.
21. Fadeev, I.G. Frictional resistance coefficient during air transport by continuous flow. *Chem. Technol. Fuels Oils* **1969**, *5*, 585–589. [[CrossRef](#)]
22. Bikbaev, F.A.; Krasnov, V.I.; Maksimenko, M.Z.; Berezin, V.L.; Zhilinski, I.B.; Otroshko, N.T. Main factors affecting gas abrasive wear of elbows in pneumatic conveying pipes. *Chem. Pet. Eng.* **1973**, *9*, 73–75. [[CrossRef](#)]
23. Sina, A.; Reza, N.H. Erosion of oval elbows in turbulent particulate natural gas flow with different aspect ratio of cross-sections. *Part. Sci. Technol.* **2019**, *39*, 150–167.
24. Gorshkov, V.I.; Verevkin, V.N.; Popov, B.G. Experimental research on particle collisions with walls of pneumatic conveying ducts. *J. Eng. Phys. Thermophys.* **1969**, *17*, 1494–1498. [[CrossRef](#)]
25. Antonín, L.; Otto, M. New approach to energetic optimization of pneumatic transport. *Chem. Eng. Process. Process Intensif.* **1990**, *28*, 95–100.
26. Li, J.; Pandiella, S.S.; Webb, C.; McGlinchey, D.; Cowell, A.; Xiang, J.; Knight, L.; Pugh, J. An Experimental Technique for the Analysis of Slug Flows in Pneumatic Pipelines Using Pressure Measurements. *Part. Sci. Technol.* **2002**, *20*, 283–303. [[CrossRef](#)]
27. Chung, W.-S. Optimization of Waste Pneumatic Transportation System by Results of Facility Diagnosis. *J. Fluid Mach.* **2010**, *13*, 54–57. [[CrossRef](#)]
28. Behera, N.; Agarwal, V.K.; Jones, M.G. A model of solids friction factor for fluidized dense phase pneumatic conveying. *Powder Technol.* **2015**, *284*, 403–410. [[CrossRef](#)]
29. Ma, G.; Ma, H.; Sun, Z. Simulation of Two-Phase Flow of Shotcrete in a Bent Pipe Based on a CFD-DEM Coupling Model. *Appl. Sci.* **2022**, *12*, 3530. [[CrossRef](#)]
30. Liu, W.; Chen, G.; Liu, C.; Zheng, D.; Ge, M. Experimental and Numerical Study of Pressure Drop Characteristics of Soybean Grain under Vertical Pressure. *Appl. Sci.* **2022**, *12*, 6830. [[CrossRef](#)]
31. Xue, R.; Lin, X.; Zhang, B.; Zhou, H.; Lai, T.; Hou, Y. CFD and Energy Loss Model Analysis of High-Speed Centrifugal Pump with Low Specific Speed. *Appl. Sci.* **2022**, *12*, 7435. [[CrossRef](#)]

32. Ghafari, H.; Sharifi, M. Numerical and experimental study of an innovative design of elbow in the pipe line of a pneumatic conveying system. *Powder Technol.* **2018**, *331*, 171–178. [[CrossRef](#)]
33. Wang, Y.; Williams, K.; Jones, M.; Chen, B. CFD simulation methodology for gas-solid flow in bypass pneumatic conveying—A review. *Appl. Therm. Eng.* **2017**, *125*, 185–208. [[CrossRef](#)]
34. Ghafari, H.; Ebrahimi, H.R. Numerical and experimental study of an innovative pipeline design in a granular pneumatic-conveying system. *Particuology* **2018**, *38*, 196–203. [[CrossRef](#)]
35. Yang, D.; Li, G.; Wang, Y.; Wang, Q.; Li, J.; Huang, Q.; Xia, Y.; Li, Q. Prediction of Horizontal Pneumatic Conveying of Large Coal Particles Using Discrete Phase Model. *Adv. Mater. Sci. Eng.* **2020**, *2020*, 1967052. [[CrossRef](#)]
36. Kuang, S.; Li, K.; Yu, A. CFD-DEM Simulation of Large-Scale Dilute-Phase Pneumatic Conveying System. *Ind. Eng. Chem. Res.* **2019**, *59*, 4150–4160. [[CrossRef](#)]
37. Yang, L.; Xie, Y.H. *Pneumatic Conveying Engineering*, 1st ed.; China Machine Press: Beijing, China, 2006; pp. 79–89.
38. Li, S.J.; Zhou, X.J. *Theory and Application of Pneumatic Conveying*, 1st ed.; China Machine Press: Beijing, China, 1992; pp. 49–68.
39. Kalman, H.; Satran, A.; Meir, D.; Rabinovich, E. Pickup (critical) velocity of particles. *Powder Technol.* **2005**, *160*, 103–113. [[CrossRef](#)]
40. Fu, P.; Liu, L.H.; Yang, W.P.; Liu, R.X.; Zhang, K.; Guo, W.L.; Leng, C.Q. Design and experiment of Pneumatic conveying system for feed. *J. Heilongjiang Anim. Husb. Vet. Sci.* **2021**, *24*, 76–82+147.
41. Wang, Z.Q.; Su, H.H. Simplified derivation of Stokes Viscosity Resistance Formula. *J. Univ. Electron. Sci. Technol. China* **1997**, *26* (Suppl. S1), 261–264.
42. Cabrejos, F.J.; Klinzing, G.E. Incipient motion of solid particles in horizontal pneumatic conveying. *Powder Technol.* **1992**, *72*, 51–61. [[CrossRef](#)]
43. Zhang, G.Q.; Wu, J.M. *Fluid Mechanics*, 1st ed.; China Machine Press: Beijing, China, 2006; pp. 52–70.
44. Peng, F.; Wang, H.Y.; Fang, F.; Liu, Y.D. Parameter calibration of granular feed discrete element Model based on injection cross section method. *Trans. Chin. Soc. Agric. Mach.* **2018**, *49*, 140–147.

Disclaimer/Publisher’s Note: The statements, opinions and data contained in all publications are solely those of the individual author(s) and contributor(s) and not of MDPI and/or the editor(s). MDPI and/or the editor(s) disclaim responsibility for any injury to people or property resulting from any ideas, methods, instructions or products referred to in the content.